Influence of variable hydrodynamic interaction strength on the transport properties of coiled polymers

Marc L. Mansfield*,†
Department of Chemistry, Chemical Biology, and Biomedical Engineering, Stevens Institute of Technology, Hoboken, New Jersey 07030, USA

Jack F. Douglas*,‡
Polymers Division, National Institute of Standards and Technology, Gaithersburg, Maryland 20899, USA
(Received 28 July 2009; published 19 February 2010)

We have computed the hydrodynamic radius R_h and intrinsic viscosity $[\eta]$ of a large number of random coil polymer models by path integration. We examine the effects of chain length, solvent quality, monomer size and shape, and chain stiffness on the approach of these transport properties to the limit of large molecular mass. For many of the models, we have also calculated the ensemble-averaged solvent velocity field in the vicinity of the coil as it moves with constant drift velocity under the action of an external force. Naive scaling arguments predict $\alpha=\nu$ and $\beta=3\nu-1$, where α, β, and ν are the exponents controlling the chain length behavior of R_h, $[\eta]$, and R_g, respectively. We present evidence for a "draining crossover" that quantifies the slow convergence of the transport properties to their asymptotic scaling behavior. Indeed, the convergence is so slow that effective α and β exponents rarely agree with the naive predictions at typical molecular masses. For the same chain models, R_g converges rapidly to its asymptotic behavior, indicating that the effect is not due to a crossover from theta to swollen behavior, as often stated. Solvent quality, monomer size, and chain stiffness all influence the draining crossover. Our results call into question the common practice of extracting metrical data, e.g., characteristic ratios, directly from polymer solution transport properties.

DOI: 10.1103/PhysRevE.81.021803 PACS number(s): 83.80.Rs, 66.20.Cy, 66.10.cg

I. INTRODUCTION

The transport properties of polymers are important both in molecular characterization and in understanding the kinetic properties of many time-dependent solution processes. Due to recent advances in the computation of transport properties [1–15], we are in a position to predict a number of transport properties of particles of any shape to unprecedented accuracy. Here, we present a numerical study of the scaling laws of the hydrodynamic radius and the intrinsic viscosity of random coil chains as a function of chain geometry. In particular, we examine the influence of solvent quality, monomer structure, and backbone flexibility on solution transport properties such as the hydrodynamic radius and the intrinsic viscosity. We are particularly interested in how the size and shape of monomers and the chain stiffness affect the approach of these solution properties to the infinite-chain scaling limit.

It is well known that the static properties of linear polymers follow universal size-scaling laws in the long-chain limit [16,17],

$$R_g \sim N^{\nu}, \tag{1}$$

where R_g is the radius of gyration, N is the number of chain segments, and ν is a universal exponent. Two different classes of models have been utilized for studying linear polymers [16,17]. The first of these, the so-called ideal chains, are patterned after the standard random walk, and neglect all interactions between segments that are not proximal along the chain contour. The second class, which we refer to here as "real" chains, incorporate realistic interactions between all pairs of segments, including both a bare repulsive excluded-volume interaction and an attractive component that permits us to tune the solvent quality. All ideal chains belong to the same universality class, characteristic of random walks, with $\nu=1/2$ and with Gaussian end-end distributions. However, for real chains there are three separate universality classes depending on the balance between attractive and repulsive interactions. First, when repulsions dominate, we have the "self-avoiding random walk" or "good solvent" scaling exponent, $\nu\cong 0.588$, for equilibrium solution properties [18]. Second, if attractions dominate, then the solvent is so poor that the chain collapses to a globule and $\nu=1/3$. Third, if attractions and repulsions are compensatory, then we have the theta-state for which $\nu=1/2$ in three dimensions. Even though they are less realistic, ideal chain models provide a useful reference model for two reasons. First, they are more tractable and, second, the generally accepted wisdom is that they are reasonable representations of the long-range properties of theta-state chains in three spatial dimensions.

According to classical scaling arguments for polymer solution transport properties, we expect the diffusion coefficient D, the friction coefficient f, and the intrinsic viscosity $[\eta]$ to follow scaling laws of their own [16],

$$D^{-1} \sim f \sim N^{\alpha}, \quad [\eta] \sim N^{\beta}, \tag{2a}$$

*Corresponding author.
†marc.mansfield@stevens.edu
‡jack.douglas@nist.gov

$$\alpha = \nu, \quad \beta = 3\nu - 1. \tag{2b}$$

Here, ν is the same exponent that appears in Eq. (1) and β is usually referred to as the Mark-Houwink index. However, the experimental evidence supporting the universality of these exponents is weak. The effective α and β exponents are often smaller than the values cited in Eqs. (2), and it is not unusual to see exponents near 0.5 for shorter chains that approach values expected for good solvents when the chains become longer [16,19,20]. In particular, Adam and Delsanti measured the effective exponents α and ν to be about 0.55 and 0.6, respectively, for the same polymer-solvent system [21]. The equivalent effect for the intrinsic viscosity is probably better known. Scaling theory predicts $\beta \approx 0.77$ under good solvent conditions. However, the empirical Mark-Houwink exponents for flexible chains are normally smaller than this, even in good solvents [19,22].

One interpretation is that these deviations are manifestations of a crossover from theta to good solvent conditions. Short chains are assumed to be in an effective theta-state since the chains are not long enough to have appreciable self-excluded-volume interactions. Although we do not want to rule out this interpretation in all cases, our calculations indicate another interpretation. We find that polymer solution transport properties are particularly slow to converge to the infinite-chain limit. For any property, finite-length corrections to universal behavior depending on local details such as monomer shape or backbone flexibility can always be expected. The question is how rapidly these corrections to scaling disappear from either the metric data, i.e., R_g, or from the transport data, i.e., R_h and $[\eta]$. This paper presents calculations on the transport properties of both ideal and real chain models with a variety of monomer shapes and backbone flexibility. We find that convergence to the infinite-chain limit is so slow for transport properties that convergence of the exponents to their asymptotic limits does not occur for typical synthetic polymers at typical molecular weights. For example, deviations of the exponents for some models are still obvious at a polymerization index of $N=10^4$. A polystyrene chain of 10^4 monomers has a molecular mass greater than 10^3 kg/mol, which is larger than most commercially available polystyrenes. In other words, many synthetic polymers are simply too short to conform to the scaling relations of Eqs. (2).

These gradually changing effective exponents for transport properties are manifestations of what is usually called the "hydrodynamic draining" effect and have been observed in other approximate models of the transport properties of random coils. For example, the effect of monomer size and shape enters the Kirkwood-Riseman theory [19,23,24] and other later developments such as the Rouse-Zimm model [25,26] through the monomer friction coefficient. Wang and co-workers examined the problem in several renormalization-group studies [27–31]. The main purpose of this paper is to examine the slow convergence of transport properties to their long-chain asymptotic behavior using other numerical techniques.

Our understanding of the transport characteristics of random coils is based on a consideration of the strength of the hydrodynamic interaction of the random coil with the solvent. Because of the no-slip boundary condition, a random coil polymer transporting through a quiescent solvent induces a flow field in the solvent which equals the polymer velocity near the polymer and which decays to zero at large distances. In the so-called "nondraining" approximation, it is argued that the polymer drags with it a "blob" of solvent. The spatial extent of the blob is proportional to R_g (there being no other length scale in the problem) and scaling laws such as Eqs. (2) result. We are now able to accurately calculate this velocity flow field for arbitrary polymer models. As we will show, the solvent velocity profile depends on the size and shape of the monomer units, on the chain stiffness, and on the solvent quality. This velocity profile eventually converges to its $N \to \infty$ form, which depends on distance r from the center of mass entirely as a function of r/R_g. Obviously, at the same large N values, the ratio R_h/R_g also reaches its large-N limit. We find that the trends in the draining characteristics of any given polymer are consistent with expectations: theta chains are less "draining" than swollen chains, and either decreasing the monomer size or increasing the chain stiffness makes the coil more draining. However, the notion that the flow field saturates monotonically to some nondraining limit as $N \to \infty$ is oversimplified. According to our calculations, many polymers are more draining in the $N \to \infty$ limit than they are at finite N. Equivalently, the R_h/R_g ratio can approach its $N \to \infty$ limit from either above or below. Obviously, until R_h/R_g reaches its limit, effective exponents appearing in Eq. (2a) can be either *larger* or *smaller* than the predictions given in Eq. (2b).

We calculate the velocity field, as well as all other transport properties, in the so-called "electrostatic approximation." A common approach in hydrodynamic calculations is to replace the complete Oseen tensor with its angular average. Since this average is proportional to $1/r$, or the electrostatic Green's function, many hydrodynamic problems have direct analogs in electrostatics. The hydrodynamic radius and intrinsic viscosity are, respectively, analogous to the electrostatic capacity and electrostatic polarizability tensor of a perfect conductor having the same size and shape as the object in question, while the velocity field is analogous to the electrostatic potential of a charged perfect conductor having the same size and shape as the polymer. The computation takes the form of a path integration, which simultaneously gives, within the electrostatic approximation, the electrostatic and the transport properties [1–15]. The approximation has an uncertainty that is normally better than 1% or 2% for the hydrodynamic radius and the intrinsic viscosity, respectively, for particles of general shape [15].

Weill and des Cloizeaux [20] also interpreted this crossover effect in terms of a slow convergence to asymptotic behavior, and our results accord qualitatively with many of their arguments, despite the fact that their arguments were not based on a reliable hydrodynamic theory. Specifically, their analysis is based on an argument that the dimensionless ratio $m[\eta]_P/R_g^2 R_h$ is the same for all random coils. This assertion is not supported by our calculations. Moreover, we find that the ratio $m[\eta]_P/R_h^3$ displays less variability among macromolecules, including random coils, than the ratio that they propose.

The path-integration technique gives a direct estimate of the hydrodynamic radius R_h, from which the diffusivity D and the friction coefficient f can be computed,

$$D = \frac{kT}{6\pi\eta_0 R_h}, \tag{3}$$

$$f = 6\pi\eta_0 R_h. \tag{4}$$

Here k, T, and η_0 are, respectively, the Boltzmann constant, temperature, and solvent viscosity. The path-integration technique also gives a direct estimate of the hydrodynamic volume V_h, which is related to the intrinsic viscosity $[\eta]$ or $[\eta]_P$,

$$V_h = \tfrac{2}{5}V[\eta] = \tfrac{2}{5}m[\eta]_P. \tag{5}$$

Here, V and m are, respectively, the volume and mass of the particle. Two different conventions for defining the intrinsic viscosity are encountered in the literature. For clarity, therefore, we use two different symbols: $[\eta]$ is dimensionless, while $[\eta]_P$, the "practical" intrinsic viscosity, has dimensions of volume/mass and is the definition most commonly encountered in experimental polymer science. The intrinsic viscosity is the leading virial coefficient of the solution viscosity. In other words, we have

$$\eta = \eta_0(1 + [\eta]_P c + \cdots) \tag{6a}$$

or

$$\eta = \eta_0(1 + [\eta]\phi + \cdots), \tag{6b}$$

where η and η_0 are, respectively, the solution and solvent viscosities, and where c and φ are, respectively, the mass concentration and the volume fraction of the solution. All theories and computations of the intrinsic viscosity (including ours) directly determine V_h. The intrinsic viscosity is obtained secondarily by normalization with either the volume or the mass through Eq. (5). Here, we will follow the convention of normalizing by the mass and assume mass units such that an individual monomer has unit mass. Therefore,

$$m = N \quad \text{or} \quad m = (1.5)N \tag{7}$$

for our models, where N is the number of backbone segments. (Some models carry $N/2$ side groups in addition to the N backbone segments; for these, $m=1.5N$. See below.) The path-integral formalism also lets us calculate the ensemble-averaged solvent velocity profiles mentioned above.

II. IDEAL CHAIN MODELS

We have calculated the transport properties of both ideal chains (i.e., chains without long-range excluded-volume interactions) and real chains. All chain models have been constructed on the simple-cubic lattice, with length units such that the lattice spacing is 1. This section describes the ideal chain models, while real chains are introduced in the following section. We considered a number of different chain ensembles with different statistical properties in order to examine the effects of chain stiffness. Let $\boldsymbol{r}_j$ represent the lattice site occupied by the jth segment of the chain, with $0 \le j \le N-1$, so that N is the number of segments in the chain. Let

$$\boldsymbol{v}_j = \boldsymbol{r}_j - \boldsymbol{r}_{j-1} \tag{8}$$

represent the displacement vector between two successive segments. There are $N-1$ of the $\boldsymbol{v}_j$'s, with $1 \le j \le N-1$. Because these are lattice walks, each $\boldsymbol{v}_j$ is one of six different unit vectors, $\pm\boldsymbol{e}_x, \pm\boldsymbol{e}_y, \pm\boldsymbol{e}_z$. Beginning at the origin, $\boldsymbol{r}_0=0$, the first step is taken at random to be any of these six lattice vectors. For each step of the walk after the first, with probability p_f, we place segment j such that $\boldsymbol{v}_j$ is parallel to $\boldsymbol{v}_{j-1}$. With probability p_b, we place it such that $\boldsymbol{v}_j$ and $\boldsymbol{v}_{j-1}$ are antiparallel (which also means that segment j is placed at the same lattice site as segment $j-2$), and with probability p_o, it is placed in any one of the four remaining directions. (The three subscripts represent "forward," "backward," and "orthogonal," and since we have no other options, $p_b+p_o+p_f=1$.) Whenever an orthogonal step is taken, any one of the four steps is chosen with equal probability. Such chains have correlations between successive steps ("step correlations"), which decay exponentially

$$\langle \mathbf{v}_i \cdot \mathbf{v}_j \rangle = g^{|j-i|}, \tag{9}$$

where

$$g = p_f - p_b. \tag{10}$$

The characteristic ratio of each model is given by [32]

$$C = \frac{1+g}{1-g} \tag{11}$$

and characterizes the stiffness of the chain.

In this work, we analyzed eight different examples of ideal chain models, differing in the values of (p_b, p_o, p_f). Table I summarizes the properties of the different models. Model **r** consists of standard six-choice random walks on the simple-cubic lattice in which each step is taken in an entirely random direction independent of all other steps, and therefore exhibits no step correlation ($g=0$) and has characteristic ratio $C=1$. Model **t** only permits orthogonal steps, and therefore also has $g=0$ and $C=1$. The models designated **u**, **v**, **a**, **q**, and **w** all eliminate back steps ($p_b=0$) but have different values of p_f and therefore differing characteristic ratios and differing chain stiffnesses. Model **x** eliminates the forward step but has a rather large probability of taking a backward step and, therefore, has a small characteristic ratio and a very large volume overlap. Nevertheless, it is expected to approach the same universality class as all the other ideal chains and is included here in an attempt to observe convergence to universality in an unusual class of chains. Transport properties and gyration radii were evaluated for all of these models by our path-integration technique for N values from 30 to about 6×10^4. The radius of gyration R_g can be computed exactly for these models, with the required formula given in the supplementary material accompanying this paper [33], and agrees well with the values computed by simulation.

TABLE I. Characteristics of the ideal model chains considered here. Effective exponents ν, α, and β were calculated in the range $10^{2.7}<N<10^{3.5}$.

Model code	(p_b,p_o,p_f)	g	C	d	ω	τ	ν	α	β
w	$\left(0,\frac{1}{5},\frac{4}{5}\right)$	$\frac{4}{5}$	9	$-\frac{20}{3}$	−5.31	−94.9	0.501	0.539	0.587
q	$\left(0,\frac{1}{3},\frac{2}{3}\right)$	$\frac{2}{3}$	5	$-\frac{18}{5}$	−2.51	−40.3	0.495	0.513	0.524
a	$\left(0,\frac{1}{2},\frac{1}{2}\right)$	$\frac{1}{2}$	3	−2	0.188	10.2	0.501	0.500	0.503
v	$\left(0,\frac{2}{3},\frac{1}{3}\right)$	$\frac{1}{3}$	2	$-\frac{9}{8}$	1.79	43.3	0.498	0.486	0.466
u	$\left(0,\frac{4}{5},\frac{1}{5}\right)$	$\frac{1}{5}$	$\frac{3}{2}$	$-\frac{5}{8}$	2.17	50.8	0.504	0.481	0.454
r	$\left(\frac{1}{6},\frac{2}{3},\frac{1}{6}\right)$	0	1	0	4.07	90.7	0.499	0.470	0.427
t	(0,1,0)	0	1	0	3.97	87.5	0.501	0.469	0.423
x	$\left(\frac{2}{3},\frac{1}{3},0\right)$	$-\frac{2}{3}$	$\frac{1}{5}$	$+\frac{18}{5}$	9.70	212	0.499	0.430	0.314

III. REAL CHAIN MODELS

We have examined real chains, i.e., chains with intersegment interactions between all pairs of segments, on the simple-cubic lattice. The interaction combines a hard-core excluded volume with a nearest-neighbor contact potential. In other words, any chain for which two or more segments occupy the same lattice site is excluded from the ensemble. All other chains have Hamiltonian equal to the product of the "contact potential," $-\varphi$, and the total number of pairs of segments occupying nearest-neighbor lattice sites. Seven different model classes, **A**, **D**, **M**, **Q**, **T**, **Z**, and **C**, distinguished by the value of φ, were considered. These models are summarized in Table II. Model **T** at $\varphi=0.27$ is known to lie close to the theta point [34,35]. Models **A**, **D**, **M**, and **Q** lie above the theta point, while **Z** and **C** lie below. These self-avoiding walks were generated either only by pivoting [36] or else by a more elaborate annealing procedure [35] combining pivoting and Berg-Foerster-Aragao de Carvalho-Caracciolo-Froelich (BFACF) moves [37–39]. Snapshots of a number of such chains appear in Fig. 1.

For all of the chain models presented above, both ideal and real, individual chain segments are assumed to be a single lattice unit cell or a cube of unit volume. [Therefore, for all the models discussed above, we normalize Eq. (5) according to $m=V=N$.] An essential parameter in the Kirkwood-Riseman formalism for the transport properties of macromolecules is the friction coefficient of an individual segment, which obviously is a function of the size and shape of the segment [19,23,24]. To explore such segmental effects, we have also considered a number of models constructed by modifying the segmental structure of lattice self-avoiding walks at either $\varphi=0$ (model **A**) or 0.27 (model **T**). These modifications were made without perturbing the parent backbone structures. In this way, the segmental friction coefficients change significantly without changing the global structure of the chain. This permits us to separate out the effects due only to the structure of the individual segments.

One such modification consisted of replacing the cubical lattice cell with a sphere (or "bead") of radius b centered at the lattice site. These beads varied in radius from very small ($b=0.01$) to so large that contiguous beads overlap ($b=1$). Such models are designated **Ab**⟨**nnn**⟩ or **Tb**⟨**nnn**⟩…, with the first letter signifying the parent structure (**A** or **T**), with the letter "**b**" signifying bead, and with the suffix ⟨**nnn**⟩ encoding the bead radius (see Table II). Notice that for bead models with $b<0.5$, the chains are not simply connected and are therefore unphysical.

Another modification applied to chains of model **A** and of backbone length N was the grafting of $N/2$ additional side-group segments. These side groups were also modeled as a single unit cube and were added in such a way that all were nearest neighbors of some segment in the backbone. Then the side groups were annealed subject to three constraints: (1) the backbone was maintained rigidly, i.e., it was generated *a priori* as some instance of model **A** at length N, and its structure did not vary upon the addition, or during the annealing, of the side groups. (2) Volume exclusion between all segments, both side groups and backbone, was enforced. (3) Any side group was required to be the nearest neighbor of some segment in the backbone. This model is designated **As**, with the "**s**" signifying "side groups." In other words, for model **As**, each backbone segment is again a unit cube, and 50% of these backbone segments also carry a side group, also represented as a unit cube. We continue to let N represent the length of the backbone, so these models consist of $1.5N$ individual lattice cubes.

The model class **Ar** is comprised of self-avoiding ring polymers. These were also generated on the simple-cubic lattice at $\varphi=0$ (hence the prefix "**A**"). They were generated

TABLE II. Summary of real models. If the column labeled "modification" contains the entry "none," then the model consists of self-avoiding walks on the simple-cubic lattice with the specified nearest-neighbor contact potential $-\phi$ and with each monomer represented hydrodynamically as a cubic lattice cell. Modifications consisted of either (1) replacing each cubical monomer unit with a spherical bead of the specified radius or (2) adding $N/2$ side groups each of which was also a cubic lattice cell. Models **Ar** and **Ars** are ring chains; all others are linear chains. Effective exponents ν, α, and β were calculated in the range $10^{2.7} < N < 10^{3.5}$.

Model code	ϕ	Modification	ν	α	β
A	0	None	0.586	0.564	0.708
D	0.1	None	0.590	0.556	0.692
M	0.15	None	0.575	0.546	0.657
Q	0.2	None	0.562	0.535	0.620
T	0.27	None	0.510	0.490	0.482
Z	0.35	None	0.109	0.252	–0.303
C	0.5	None	0.282	0.304	–0.096
Ab01		**A**, beads, 0.01	0.589	0.833	1.064
Ab025		**A**, beads, 0.025	0.589	0.733	0.997
Ab05		**A**, beads, 0.05	0.589	0.673	0.910
Ab1		**A**, beads, 0.1	0.589	0.629	0.843
Ab2		**A**, beads, 0.2	0.589	0.603	0.793
Ab25		**A**, beads, 0.25	0.589	0.590	0.772
Ab5		**A**, beads, 0.5	0.594	0.570	0.737
Abo		**A**, beads, 1.0	0.589	0.548	0.677
Tb01		**T**, beads, 0.01	0.504	0.761	0.881
Tb025		**T**, beads, 0.025	0.504	0.654	0.768
Tb05		**T**, beads, 0.05	0.504	0.590	0.680
Tb1		**T**, beads, 0.1	0.504	0.549	0.618
Tb25		**T**, beads, 0.25	0.504	0.513	0.552
Tb5		**T**, beads, 0.5	0.504	0.495	0.507
Tbo		**T**, beads, 1.0	0.504	0.473	0.442
Ar	0	None	0.589	0.569	0.716
Arb2		**Ar**, beads, 0.2	0.591	0.598	0.790
Arb5		**Ar**, beads, 0.5	0.594	0.573	0.730
As		**A**, side groups	0.596	0.546	0.678
Ars		**Ar**, side groups	0.593	0.548	0.661

by pivoting of linear chains, taking every tenth instance of a linear for which segments 1 and N are nearest neighbors as one instance of a ring chain [40]. The ring polymers of designation **Ar** were also submitted to the segmental modifications described above, producing models **Ar2** and **Ar5** when beads replaced lattice cells, and model class **Ars** when the rings were adorned with $N/2$ side groups. Table II gives a full list of the models considered and summarizes the details about their generation.

The segmental structure is, of course, a nonuniversal local property, and so its effect should disappear from all long-range properties. However, as we will see below, as one example of a hydrodynamic draining effect, it continues to influence the transport properties even at large molecular weights.

For the models **As** and **Ars**, we assume $m=1.5N$ in normalizing the intrinsic viscosity. For all other models, we take $m=N$. Obviously, the total chain volume varies significantly as the structure of the segment is modified [41]. Because the generation of chains with long-range interactions requires annealing, the real chain models have only been studied, for the most part, out to $N \approx 2000$, with the annealing procedures explained above. The approach for generating rings guarantees unbiased sampling of self-avoiding rings [40], including rings of all possible knot states. However, at these chain lengths, knots are known to be extremely rare in the full ensemble of self-avoiding rings [42]. Therefore, the ring chains examined here are essentially unknotted. In another work, we will present results on the transport properties of self-avoiding rings with knots.

IV. DRAINING CHARACTERISTICS OF VARIOUS POLYMER MODELS

The term draining signifies the extent to which the solvent is able to flow through the transporting polymer coil without

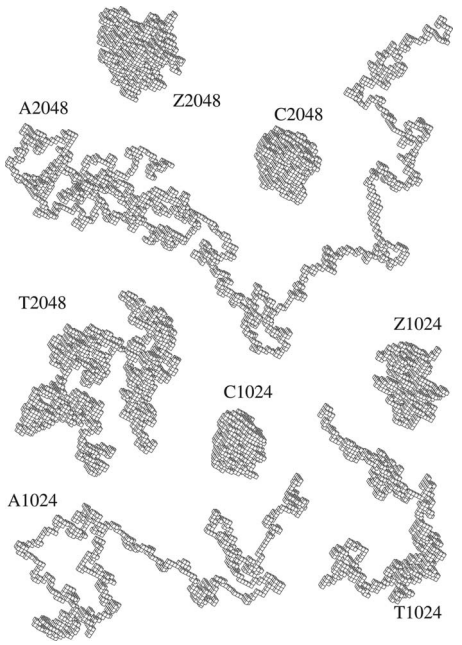

FIG. 1. Projections of several realizations of lattice model chains. The label "Z2048" indicates an example of model **Z** of length 2048 segments, etc.

being perturbed, or penetration of the velocity field into the region of the polymer. Equivalently, it represents the absence of "hydrodynamic screening." As mentioned above, the flow field is analogous to the electrostatic potential of a charged conductor of the same shape. Therefore, we determine the function Φ which equals 1 everywhere over the surface and inside the polymer particle, which decays to zero at large distances, and which satisfies the Laplace equation everywhere outside the particle. We plot $\langle\Phi\rangle$ as a function of the distance from the center of mass, where the angular brackets denote an average over all orientations and conformations of the flexible chain. (Conformational ensemble averages are computed over 1000 statistically independent samples.) A number of these curves are shown in Figs. 2 and 3. Equivalently, these curves represent the ensemble-averaged velocity field in the fluid in the vicinity of the particle, under the assumption that the particle has unit drift velocity [1]. Let r_{max} be sufficiently large that a sphere of radius r_{max} completely circumscribes the polymer in all its conformations. Then for any $r > r_{max}$, we have

$$\langle\Phi\rangle = R_h/r, \tag{12}$$

which is exact within the electrostatic approximation [33]. Of course, we observe departures from Eq. (12) at smaller r and, indeed, $\langle\Phi\rangle$ can never be greater than 1. The results of Eq. (12) appear as dashed lines in Fig. 2. In other words, R_h determines the rate of decay of the hydrodynamic disturbance about the particle.

For rigid spheres of radius R, we have [33]

$$\langle\Phi\rangle = 1 \quad \text{if} \quad r < R, \tag{13a}$$

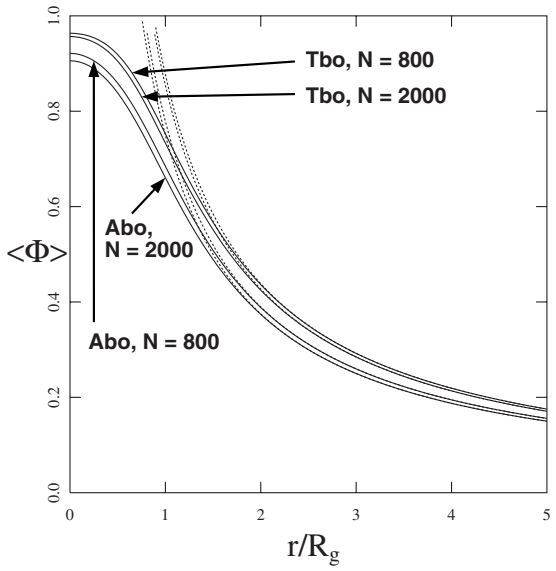

FIG. 2. Angularly averaged profiles of the solvent flow field induced in the vicinity of a random coil having unit drift velocity are shown here for models **Abo** and **Tbo** at chain lengths of both 800 and 2000. The quantity r is the distance from the center of mass of the polymer. The flow field behaves like R_h/r at large distances, for R_h the hydrodynamic radius, which behavior is shown here with the dashed curves. The theta-state polymers (**Tbo**) are less draining than the swollen polymers (**Abo**).

$$\langle\Phi\rangle = R/r \quad \text{if} \quad r > R. \tag{13b}$$

We also expect, at large enough N, for the polymers to enter an asymptotic scaling regime for which

$$\lim_{N\to\infty}\langle\Phi\rangle = f_\infty(r/R_g) \tag{14}$$

for f_∞ a universal function, independent of N. This explains our motivation for plotting $\langle\Phi\rangle$ in Figs. 2 and 3 as a function

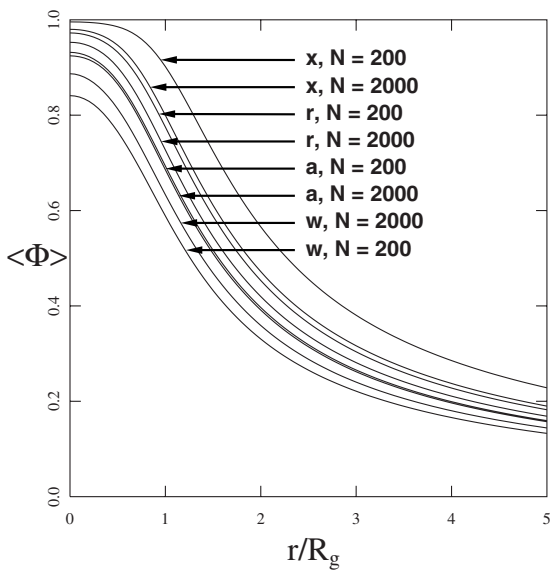

FIG. 3. Same as Fig. 2 except for ideal chain models **w**, **a**, **r**, and **x**. Stiff chains are more draining than flexible chains.

of r/R_g. Figure 2 shows results for both the **Tbo** and **Abo** models, at two different N values. Note that $\langle\Phi\rangle$ is larger for the theta chain model **Tbo**, which illustrates the general property that theta chains are less draining than swollen chains. Figure 3 shows results for ideal chains of varying stiffnesses and models **w**, **a**, **r**, and **x**, again at two different N values. Figure 3 demonstrates that stiffer chains are more draining.

Even though we expect universal behavior at large enough N [Eq. (14)], the curves drawn in Fig. 2 at $N=800$ and 2000, and in Fig. 3 at $N=200$ and 2000, are all distinguishable at the resolution of these drawings, which is the first of many examples we shall see of slow convergence to the large-N universal behavior. Furthermore, we can see that some models approach the limiting f_∞ function from above while others approach it from below. In other words, some models become more draining, and some become less, as $N\to\infty$. Of particular interest are the eight curves in Fig. 3. We expect all ideal chains eventually to converge to the same limiting f_∞ function. Models **x** and **r** are obviously trending downward, model **w** is trending upward, and model **a** is relatively stationary. Below, we present additional evidence indicating that model **a** is particularly close to the $N\to\infty$ limit, and therefore we assert that the curve shown for model **a** at $N=2000$ is probably a good representation of the f_∞ function for all ideal chains.

These figures also indicate that the classic notion of chains saturating to a nondraining limit at large N is not entirely correct. The nondraining limit would correspond to Eq. (13) and to the dashed curves in Fig. 2 since these are expected for a "hydrodynamically equivalent sphere" or a solid sphere which has the same hydrodynamic radius as the particle under consideration. These curves indicate that random coils are partially draining at all values of N and, furthermore, as we will see below, that flexible polymers drain more at large N than they do when N is small. On the other hand, the most important results of this classic notion, namely, that $R_h\sim R_g$ and $[\eta]\sim R_g^3/N$, are still asymptotically correct since R_g is the only relevant length scale.

Another useful indicator of draining behavior is the "penetration function" $\rho(r)$, the ensemble-averaged distribution of surface stresses. [In the electrostatic analogy, $\rho(r)$ is the average surface charge density.] We discarded our raw integration data before we were able to directly calculate $\rho(r)$ for any of these models. However, we have the following expression relating $\rho(r)$ and $\langle\Phi\rangle$ [33]:

$$4\pi r^2\rho(r) = -\frac{\partial}{\partial r}\left[r^2\frac{\partial\langle\Phi\rangle}{\partial r}\right], \tag{15}$$

and we can still estimate $\rho(r)$ by numerical differentiation of the $\langle\Phi\rangle$ curves. Note that, according to Eqs. (12) and (15), we have

$$\rho(r) = 0 \quad \text{for} \quad r > r_{max}, \tag{16}$$

as expected. Also, we have [33]

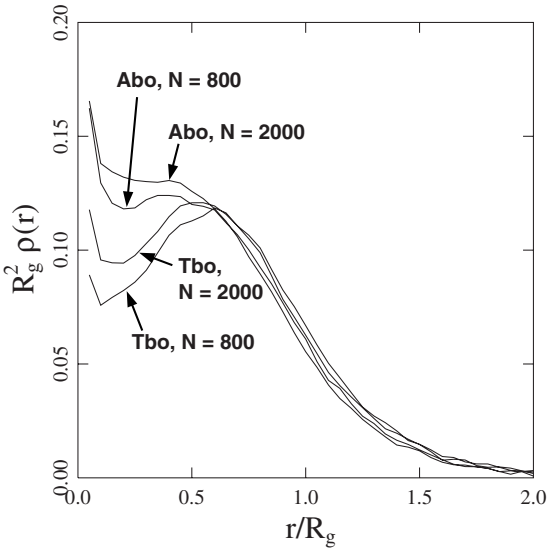

FIG. 4. The ensemble-averaged surface stresses, as a function of distance from the center of mass, which are exerted on a polymer as it moves with constant drift velocity, for the indicated models.

$$\int_0^\infty 4\pi r^2\rho(r)dr = R_h. \tag{17}$$

Finally, for a sphere of radius R, we have [33]

$$4\pi r^2\rho(r) = R\,\delta(R-r), \tag{18}$$

as expected, where δ represents the Dirac-delta function.

As defined, $\rho(r)$ has dimensions (length)$^{-2}$. Therefore, we expect $R_g^2\rho(r)$ to become a universal function of r/R_g as $N\to\infty$. Figures 4 and 5 display $R_g^2\rho(r)$ as a function of r/R_g for all of the same models considered in Figs. 2 and 3. It is again obvious from Fig. 4 that the theta coils are less draining than

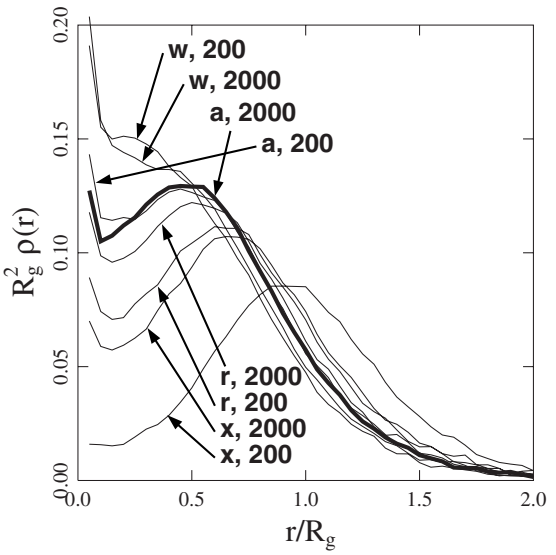

FIG. 5. Same as Fig. 4 for the indicated models. The curve for model **a** at $N=2000$ (rendered as a bold line) is especially close to the $N\to\infty$ limit of all ideal chains.

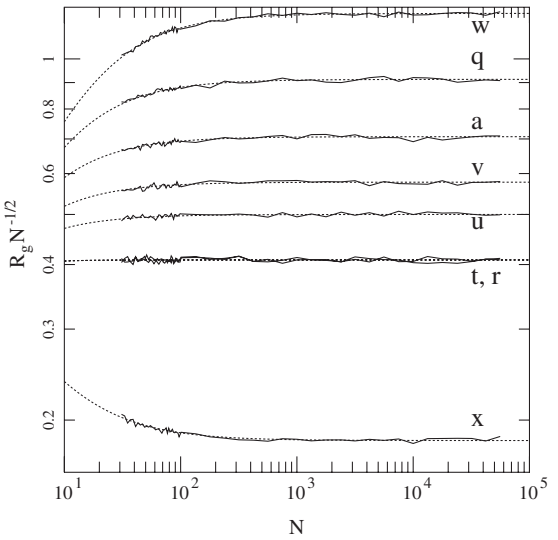

FIG. 6. Double-logarithmic plot of $R_g N^{-1/2}$ vs N for ideal chain models. Solid curves are the simulation results; dashed curves are drawn according to formulas given in the supporting information. The curvature at small N is caused by non-Gaussian contributions arising from chain stiffness.

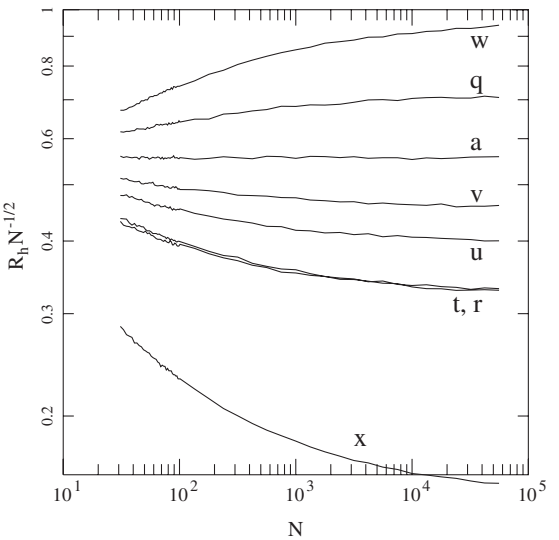

FIG. 7. Double-logarithmic plot of $R_h N^{-1/2}$ vs N for ideal chain models. Most models are only beginning to enter the asymptotic regime at $N=10^4$.

the swollen coils, while Fig. 5 again demonstrates that stiffer chains are more draining than flexible chains.

As already mentioned, all ideal chains are expected eventually to converge to a single universal curve as $N\to\infty$, which is well represented by the curve for model **a** at $N=2000$. Once again, however, Fig. 5 indicates that ideal chains have generally not yet achieved the universal limit at $N=2000$. We are not as yet able to explain the existence of the relative minima appearing in many of the $\rho(r)$ functions in the vicinity of $r\approx R_g/10$. We also point out the significant difference between the $\rho(r)$ functions appearing in Figs. 4 and 5, and the expectation for spherical particles [Eq. (18)]. The concept of a nondraining limit is not supported by these calculations. Rather, random coils are partially draining at all values of N.

Equations (12) and (14) formalize the interconnection between R_g and R_h. As long as $\langle\Phi\rangle$ is still in the process of converging to f_∞, then R_h is still in the process of converging to its asymptotic scaling law. Furthermore, whenever $\langle\Phi\rangle$ tends to f_∞ from above, we should expect that R_h depends less strongly on N than does R_g, or that the effective α is smaller than ν. Of course, the opposite is true when $\langle\Phi\rangle$ tends to f_∞ from below.

Figures 6–8 display $R_g N^{-1/2}$, $R_h N^{-1/2}$, and $[\eta]_p N^{-1/2}$ for the ideal chain models. Normalization by $N^{1/2}$ has the effect of subtracting 1/2 from the slope of any given curve, thereby accentuating the differences between different curves and making departures from strict scaling laws more evident. Probably the single most notable feature, when comparing all three sets of curves, is the relative lack of curvature in R_g, indicating that R_g achieves its asymptotic behavior much more rapidly than either R_h or $[\eta]_P$. Figures 9–11 display comparable data for real chain models. Since many sets of models are R_g equivalent, they are plotted together in Fig. 9 and labeled generically as **A** or **T**. Again note the relative lack of curvature in the R_g data.

Effective exponents for R_g, R_h, and $[\eta]_P$, determined for the range $10^{2.7}<N<10^{3.5}$, are given in Tables I and II. A very useful characterization of various draining effects is then obtained if we calculate the departure of each particular model from the expected scaling laws,

$$\Delta_\alpha=\alpha-\nu,\quad \Delta_\beta=\beta-(3\nu-1), \tag{19}$$

where—unless stated otherwise—we use the effective α, β, and ν values determined on the interval $10^{2.7}<N<10^{3.5}$. Figure 12 shows the variation in both Δ_α and Δ_β with the bead radius b of the various models **Ab**… and **Tb**…. Results for the lattice-cell models (**A**, **D**, **M**, **Q**, **T**, and **Ar**) and for the models with side groups (**As** and **Ars**) are also plotted alongside the bead models in Fig. 12. Of course, b is undefined for these latter models, so we have placed them in Fig.

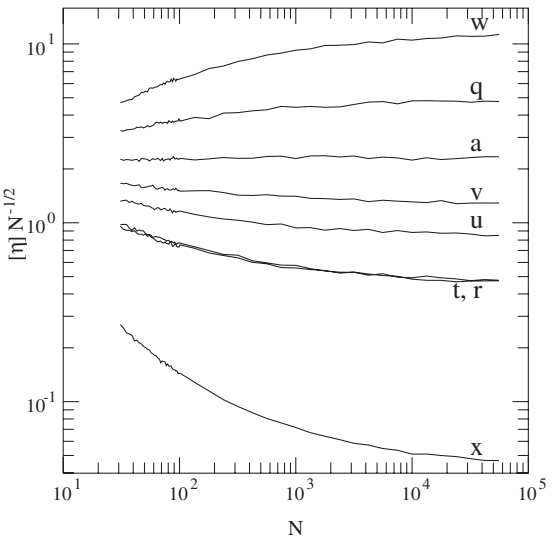

FIG. 8. Double-logarithmic plot of $[\eta]_P N^{-1/2}$ vs N for ideal chain models.

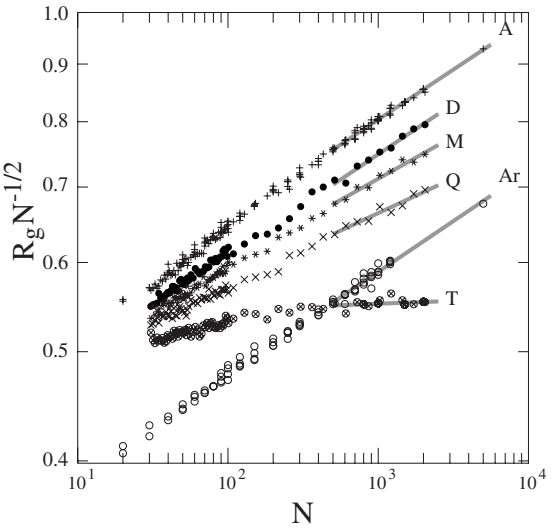

FIG. 9. Double-logarithmic plot of $R_g N^{-1/2}$ vs N for real chain models. The least-squares lines have following slopes: **A**, 0.589; **D**, 0.590; **M**, 0.575; **Q**, 0.562; **T**, 0.505; and **Ar**, 0.590.

12 at values of b (0.6 and 2.2) which appear to give reasonable agreement with the bead models. Figure 13 shows the variations in Δ_α and Δ_β for the ideal models (**w**,**q**,**a**,**v**,**u**,**r**,**t**,**x**) as functions of the characteristic ratio. As already mentioned, negative Δ_j's indicate polymer models for which $\langle\Phi\rangle$ tends to f_∞ from above, i.e., models that become more draining as $N\to\infty$, while positive Δ_j's obviously indicate the opposite. We also note the existence of compensation points in Figs. 12 and 13, at $b\approx 0.3$ and at $C\approx 3$, at which Δ_j's change sign. Obviously, such compensation points correspond to models for which $\langle\Phi\rangle$ tends to f_∞ relatively quickly, which no doubt indicates that such models have an exceptional degree of self-similarity. Model **a** lies almost precisely at one of these compensation points, which explains the relative flatness of its curves in Figs. 7 and 8. This also explains our assertion that model **a** is especially close to the universal behavior of ideal chains. We also point

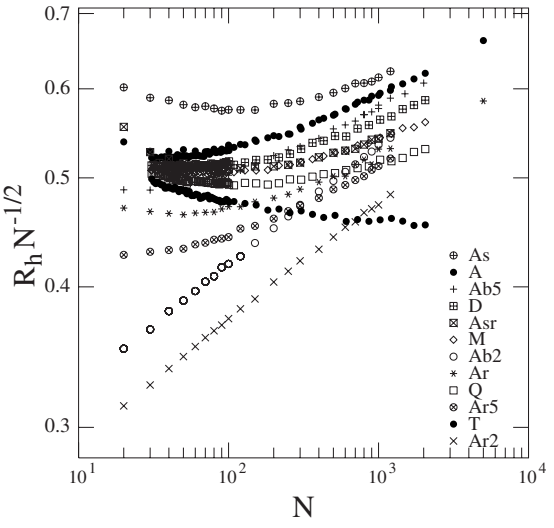

FIG. 10. Double-logarithmic plot of $R_h N^{-1/2}$ vs N for real chain models.

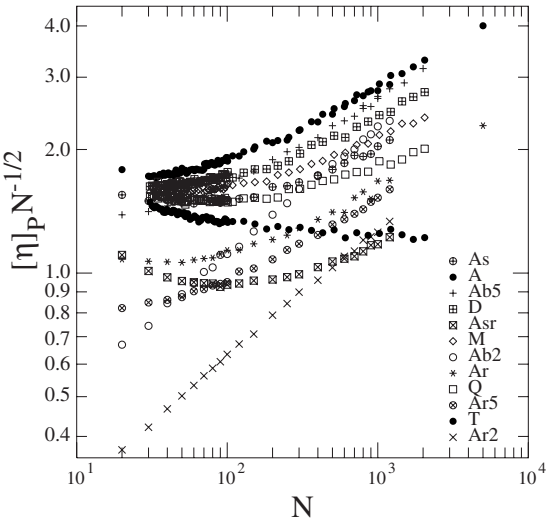

FIG. 11. Double-logarithmic plot of $[\eta]_P N^{-1/2}$ vs N for real chain models.

out that of all the models represented in Fig. 10, only those for which $b\geq 0.5$, are physically realistic, i.e., simply connected. In other words, the only flexible polymer models that could exhibit $\Delta_j>0$ are not simply connected, and so flexible chains are predicted always to display $\Delta_j<0$ and become more draining as N increases. Stiff polymers, on the other hand, can exhibit $\Delta_j>0$. This agrees well with the commonly accepted wisdom about Mark-Houwink indices [19].

V. FINITE-CHAIN CORRECTIONS TO SCALING

A complementary viewpoint of the exponent crossover is obtained by examining the following two double sums for random coil models:

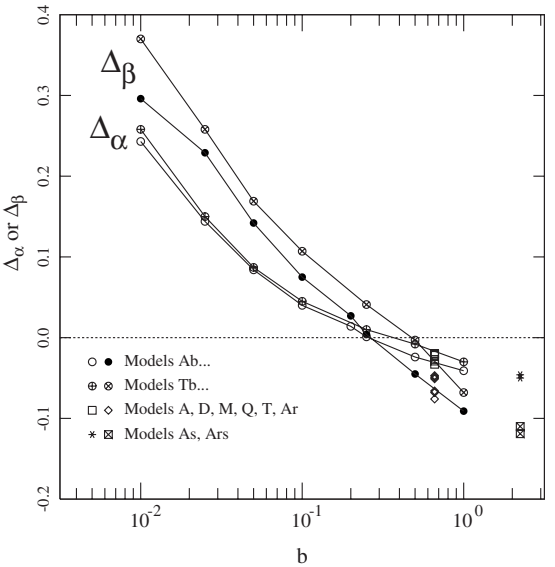

FIG. 12. Δ_α and Δ_β quantify the displacements of the effective exponents α and β away from the naive expectations of Eq. (2b). These curves display the effect of monomer shape, where b is the monomer radius.

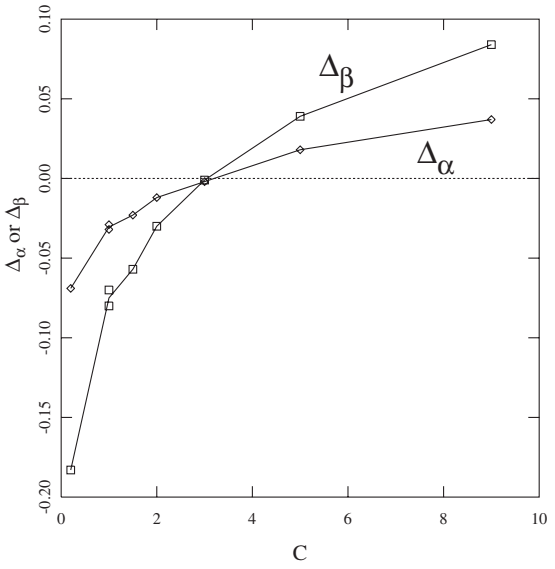

FIG. 13. Δ_α and Δ_β depend on chain stiffness. Here, C is the characteristic ratio of each of the ideal models.

$$2R_g^2 = \frac{1}{N^2}\sum_{i=0}^{N-1}\sum_{j=0}^{N-1}\langle r_{ij}^2\rangle, \tag{20}$$

$$R_K^{-1} = \frac{1}{N^2}\sum_{i=0}^{N-1}\sum_{j=0}^{N-1}\langle r_{ij}^{-1}\rangle. \tag{21}$$

The first is, of course, twice the square radius of gyration [32], while the second is the Kirkwood double-sum approximation of the reciprocal of the hydrodynamic radius [19,24,43]. The Kirkwood double-sum formula is the result of a crude preaveraging approximation and its results can be in serious error for ideal chains (displaying relative errors as large as about 20% [12]). Nonetheless, we employ it here because we anticipate that it will provide insights into the corrections to scaling of other more accurate approximations of R_h. To emphasize that Eq. (21) is a relatively poor estimate for the hydrodynamic radius, we use the notation R_K ("Kirkwood radius") for its result. We avoid the singularity at $i=j$ through the convention $\langle r_{ii}^{-1}\rangle = c$, which is equivalent, within the context of the Kirkwood formalism, to specifying a particular constant for the friction coefficient of an individual segment. The parameter c, defined in this way, serves to flag local model-dependent contributions. That is, any term depending on c is automatically recognized as being nonuniversal.

We evaluate the above sums for two different models of random coil polymers, determining not only the limiting asymptotic behavior, which is the usual focus of theoretical studies, but also finite-chain corrections to scaling. The first model is the lattice random walks introduced above as examples of ideal chains. The second is a heuristic model of real chains with a strong excluded volume. For this second model, we will assume that

$$\langle r_{ij}^2\rangle = a_2|i-j|^{2\nu} \quad \text{for all values of } i \text{ and } j, \tag{22a}$$

$$\langle r_{ii}^{-1}\rangle = c \quad \text{for all values of } i, \tag{22b}$$

$$\langle r_{ij}^{-1}\rangle = a_{-1}|i-j|^{-\nu} \quad \text{for all values of } i \neq j, \tag{22c}$$

and in all numerical studies we will assume that $\nu=0.588$. (For real chains, the front factors a_2 and a_{-1} are expected to depend on the values of i and j relative to N, but for simplicity we will ignore this here.) This second model is similar to but simpler than the one considered by Weill and des Cloizeaux [20]. In their model, ν was set equal to 1 (appropriate for stiff chains) below a first threshold, to 0.5 between that and a second threshold, and to 0.588 beyond the second threshold. For simplicity, we are effectively taking both their thresholds to be zero, which corresponds to flexible chains with a strong excluded volume. Dünweg *et al.* [44] also examined scaling corrections to Eqs. (20) and (21) for several polymer models, including beads with anharmonic (i.e., finitely extensible) springs, and report similar results.

In the supporting information [33], we obtain the asymptotic expressions and the leading correction terms for R_g and for R_K for both models. For the ideal chain model, we have

$$R_g = \left(\frac{CN}{6}\right)^{1/2}[1 + dN^{-1} + \cdots], \tag{23}$$

$$R_K = \left(\frac{3\pi CN}{128}\right)^{1/2}[1 + \gamma N^{-1/2} + \cdots]. \tag{24}$$

The leading-order result for both sums is proportional to $(CN)^{1/2}$. This is anticipated for any global measure of coil size, and it results from the assumption that the r_{ij} quantities obey Gaussian statistics. In the above expression, the coefficient d obeys

$$d = -\frac{3g}{(1-g^2)} \tag{25}$$

and therefore is model dependent. The coefficient γ is also model dependent, although we have no corresponding analytical expression. The analysis leading to Eq. (24) indicates that γ depends on the parameter $\langle r_{ii}^{-1}\rangle = c$, as well as on other local non-Gaussian terms.

For the real chain model, we have

$$R_g = (0.380)a_2^{1/2}N^{\nu}[1 + O(N^{-2})], \tag{26}$$

$$R_K = \left(\frac{0.582}{a_{-1}}\right)N^{\nu}[1 + \sigma N^{\nu-1} + \cdots], \quad \text{where } \sigma = 1.095 - 0.582\left(\frac{c}{a_{-1}}\right). \tag{27}$$

The primary difference between the results for R_g and R_K is that the corrections to scaling are of lower order for R_g, $O(N^{-1})$, or $O(N^{-2})$, than for R_K, $O(N^{-0.5})$, or $O(N^{-0.4})$, respectively. Since σ depends on c, we immediately recognize that it, like γ in Eq. (24), is nonuniversal. Obviously, R_K approaches its asymptotic behavior more slowly than does R_g. The leading terms are universal, while the correction terms include significant local contributions arising from the

TABLE III. Effective exponents of selected models when either short or long.

	ν		α		β	
Model	$N<10^{2.5}$	$N>10^{2.7}$	$N<10^{2.5}$	$N>10^{2.7}$	$N<10^{2.5}$	$N>10^{2.7}$
A	0.61	0.59	0.52	0.56	0.59	0.71
D	0.59	0.59	0.51	0.56	0.56	0.69
M	0.58	0.58	0.50	0.55	0.53	0.66
Q	0.56	0.56	0.49	0.54	0.50	0.62
T	0.53	0.51	0.47	0.49	0.43	0.48
Ab2	0.60	0.59	0.61	0.60	0.82	0.79
Ab5	0.59	0.59	0.53	0.57	0.63	0.74
Ar	0.59	0.59	0.51	0.57	0.55	0.72
Ar2	0.60	0.59	0.61	0.60	0.83	0.79
Ar5	0.59	0.59	0.53	0.57	0.62	0.73

parameter c or from when i is near j. Before we can expect universal behavior, the long-range contributions arising when i is not near j must wash out the local contributions, and this happens more slowly in the case of $\langle r_{ij}^{-1}\rangle$. The compensation points discussed above in relation to Figs. 12 and 13 correspond to situations for which γ or σ happen to be zero.

The Kirkwood radius is only an approximation to R_h [12]. Nevertheless, we are justified in expecting that correction terms for any more accurate determination of R_h are also of relative order $N^{\nu-1}$. Since the intrinsic viscosity is also determined by interactions proportional to r_{ij}^{-1}, then we can expect the same for $[\eta]_P$. It follows that R_h and $[\eta]_P$ converge to their infinite-limit scaling law more slowly than R_g.

VI. OTHER CROSSOVER EFFECTS

Table III gives effective ν, α, and β exponents for a few of the models evaluated over two different chain length regimes. It demonstrates that the effective α and β are often near 0.5 at low chain lengths and increase at higher chain lengths. However, for the same models, effective ν's are the same in both molecular-mass regimes and in Fig. 9 appear to follow the same R_g scaling law at $N\approx 30$ as at $N\approx 1000$. It has been common to attribute this effect—effective exponents around 0.5 at low molecular weights that become larger with increasing molecular weight—to a crossover from theta to good solvent conditions. Indeed, all the standard treatments of real chains, such as Flory's simple "uniform expansion" or $\alpha^3-\alpha^5$ theory, excluded-volume perturbation theory, and renormalization-group calculations, indicate that excluded-volume interactions are weaker in shorter chains [16,17,24]. However, for the models studied here, the changes in effective α and β are not accompanied by similar changes in ν. Those changes are actually due to slowly convergent, nonuniversal, and finite-chain effects in the transport properties.

Model **T**, with metric exponent $\nu\cong 0.5$, is obviously near the theta point. It also appears to accurately reproduce ideal behavior. For every property examined in this study, its behavior is always bracketed by the two ideal models **u** and **v**. For example, the best fit for its radius of gyration implies that it would lie close to an ideal chain model satisfying $g\approx 0.29$ and $C\approx 1.8$. Such an ideal chain is expected to reproduce all the global properties of the real model **T**. However, the effective α and β are below 0.5 and, on the basis of transport properties, **T** would be judged to be subtheta. Models **M** and **Q**, with effective ν's intermediate between 0.5 and 0.59, are obviously in a crossover between theta and swollen behavior. Yet they also display effective α's and β's below ν. Obviously, any crossover from theta to swollen scaling will also have, unless we happen to be at a compensation point, a hydrodynamic draining crossover superimposed upon it. This probably has far-reaching consequences for much of the polymer characterization work which has been done over the years. Much effort has gone into measuring the molecular-mass dependence of the intrinsic viscosity in order to extract information on unperturbed dimensions of polymers. However, such analyses do not take into account the draining effects discussed here. Further study seems to be required, but it would appear that determining the theta point or other conformational properties of a given polymer-solvent system solely by transport measurements may not be as accurate as has generally been believed.

VII. DIMENSIONLESS RATIOS

Certain dimensionless ratios of properties have particular interest in relation to polymer topology and shape characterization [45]. In this section, we consider some of these important ratios.

A. Ratios $\Psi_h=R_h/R_g$, $\Psi_\eta=m[\eta]_P/R_g^3$, and the Flory-Fox parameter Φ_0 for ideal chains

We let Ψ_h and Ψ_η denote, respectively, the ratio of hydrodynamic radius and radius of gyration, and the ratio of hydrodynamic volume and cube of the radius of gyration, and we let Ψ_h^* and Ψ_η^* represent the long-chain limits,

$$\Psi_h=\frac{R_h}{R_g},\quad \Psi_h^*=\lim_{N\to\infty}\Psi_h, \tag{28}$$

$$\Psi_\eta = \frac{m[\eta]_P}{R_g^3}, \quad \Psi_\eta^* = \lim_{N\to\infty} \Psi_\eta. \tag{29}$$

For ideal chains, our expectation is that both Ψ_h^* and Ψ_η^* are universal, and that there will be model-dependent corrections of amplitude $N^{-1/2}$. This expectation is confirmed, with results displayed in the supplementary material accompanying this paper [33]. Curve fitting results are as follows:

$$\Psi_h = 0.79 + \omega N^{-1/2} + \cdots \quad \text{(ideal chains)}, \tag{30}$$

$$\Psi_\eta = 6.6 + \tau N^{-1/2} + \cdots \quad \text{(ideal chains)}, \tag{31}$$

implying $\Psi_h^*=0.79$ and $\Psi_\eta^*=6.6$ for ideal chains. The coefficients ω and τ are model dependent, and their values for each of the models are given in Table I. Of course, Ψ_η^* is proportional to the Flory-Fox parameter, so our prediction for theta-state chains is

$$\Phi_0 = \lim_{N\to\infty} \frac{m[\eta]_P N_A}{(6^{1/2}R_g)^3} = 6^{-3/2} N_A \Psi_\eta^* = (2.7 \pm 0.05) \times 10^{23} \text{ mol}^{-1}. \tag{32}$$

The best empirical estimates for Ψ_h^* and Φ_0 at the theta point appear to be 0.77–0.79 and $(2.5\pm0.1)\times10^{23}$ mol^{-1}, respectively, measured for polystyrene [46–48]. Our estimate for Φ_0 is about 8% larger. However, with a characteristic ratio around 10 [32,49], polystyrene is a rather stiff chain and, as noted above, stiff chains are expected to approach Ψ_h^* and Ψ_η^* from below. Therefore, we suggest that the empirical results cited above for Ψ_h^* and Φ_0 might be slightly low because of finite-chain effects. We also suggest that with convergence controlled by $N^{-1/2}$, many polymers never reach the asymptotic domain at experimentally accessible molecular weights. In any case, it would be interesting to determine empirical values of Ψ_h^* and Φ_0 for chains more flexible than polystyrene.

The estimate of Ψ_h^* for ideal chains based on the Kirkwood double sum [Eqs. (23) and (24)] is 0.665, but this is now known to be inaccurate [12]. More recent numerical estimates based on bead-spring models without configurational preaveraging are around 0.77 [27,50,51], in rather good agreement with the present path-integral estimate. Theoretical estimates for Φ_0 include 2.66×10^{23} and 2.59×10^{23} mol^{-1} [50–52].

B. Ratios $\Psi_h=R_h/R_g$ and $\Psi_\eta=m[\eta]_P/R_g^3$ for real chains

Illustrations of Ψ_h and Ψ_η for real chains are included in the supplementary material accompanying this paper [33]. They demonstrate that, for real chains, Ψ_h^* and Ψ_η^* do not appear to be universal, with models **T**, **Q**, **M**, **D**, and **A** each appearing to extrapolate to an independent limit. For model **T** (the theta point) $\Psi_h^*=0.79\pm0.01$ and $\Psi_\eta^*=6.6\pm0.1$ (agreeing with the ideal chains, as expected). Model **A** (linear self-avoiding walk polymers) exhibits $\Psi_h^*=0.70\pm0.01$ and $\Psi_\eta^*=4.8\pm0.1$, while self-avoiding ring polymers (**Ar**) seem to be tending to limits of about $\Psi_h^*=0.85\pm0.03$ and $\Psi_\eta^*=7\pm1$. Polystyrene in good solvent conditions is reported to give Ψ_h^* values in the neighborhood of 0.63–0.69, depending on solvent [48]. Again, we speculate that this is somewhat lower than our good solvent prediction because of the inherent stiffness of the polystyrene chain.

The substantial difference in Ψ_h^* values for linear self-avoiding walks (SAWs) relative to ideal and theta chains arises from enhanced draining through the swollen chains. This has the interesting effect of reducing the errors which arise from the configurational preaveraging approximation [12]. These errors reduce from about 20% for ideal chains to about 10% for SAWs, a natural consequence of the reduced configurational fluctuations of swollen chains.

As pointed out above, we have obtained approximately the same value, $\Psi_h^*=0.79$, for both ideal and theta models. However, it should be noted that some authors [53–57] concluded that ternary excluded-volume interactions near the theta point can also contribute to R_h/R_g or to R_K/R_g. For example, Guttman *et al.* [53], obtained $R_K/R_g\cong0.71$ for self-avoiding lattice chains with nonzero contact potential, which is about 7% different from the value expected for ideal chains $(9\pi/64)^{1/2}\cong0.665$ [Eqs. (23) and (24)], while more refined calculations on larger chains by Bruns gave $R_K/R_g\cong0.683\pm0.001$ [54]. Dünweg *et al.* [44] published the value $R_K/R_g\cong0.69$ for a beads-and-springs theta model. One might invoke sampling errors and difficulties in extrapolating to infinite N in order to explain these discrepancies. However, an analytical estimate [55–57] of the ternary corrections is consistent with the simulation results. Therefore, such ternary corrections should not be discounted and are expected to complicate the crossover effects exhibited by random coil polymers, especially near the theta point. The ternary corrections should vanish in the truly infinite-chain limit, as the Brownian chain becomes an increasingly more accurate description of real polymer chains. (With a probability of 1, Brownian random flights have no triple-point intersections in three dimensions, so that three-body interactions are "irrelevant.") Nevertheless, the crossover to the asymptotic limit is predicted to be very slow [17,55–57], so that real (finite) chains under theta conditions can be expected to deviate from Gaussian chain predictions, especially in the case of transport properties.

C. Extreme values of Ψ_h and Ψ_η

We find that the values for spheres, $\Psi_h=1.291$ and $\Psi_\eta=22.53$, are exceeded both for model **x** at low N ($N<84$) and models **C** and **Z** at high N ($N>360$ and $N>2000$, respectively.) Such results can be expected for any particle with a dense core and a diffuse outer layer, because if the outer layer is neither too diffuse nor too concentrated, then it can make a significant contribution to R_h or V_h but not to R_g. Such a radial density distribution is displayed by all three models, although as previously noted, model **x** is unphysical. This result for models **C** and **Z** indicates that values of Ψ_h and Ψ_η in excess of the spherical value can be anticipated for partially collapsed chains. We are aware of one measurement which also displays this result [58].

D. Other ratios: $X_1=\Psi_h/\Psi_\eta=m[\eta]_P/R_g^2R_h$, $X_2=\Psi_h/\Psi_\eta^3=m[\eta]_P/R_h^3$, and $R_\eta/R_h=(3\Psi_h/10\pi)^{1/3}(1/\Psi_\eta)$

It has been suggested by Weill and des Cloizeaux [20] that the dimensionless ratio

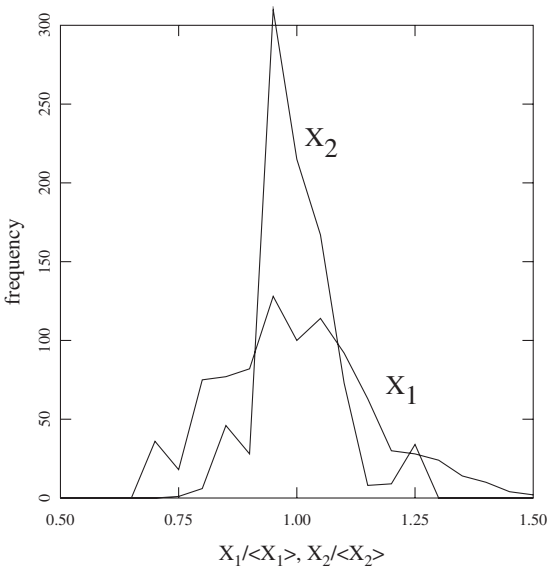

FIG. 14. Distributions of the quantities $X_1/\langle X_1\rangle$ and $X_2/\langle X_2\rangle$ over all the random coil models considered in this study.

$$X_1 = \frac{\Psi_h}{\Psi_\eta} = \frac{m[\eta]_P}{R_g^2 R_h} \tag{33}$$

takes on a universal value for all random coils. For infinitely long ideal and theta chains, this ratio is about 8.3. However, the ratio

$$X_2 = \frac{\Psi_h}{\Psi_\eta^3} = \frac{m[\eta]_P}{R_h^3} \tag{34}$$

(which assumes the value of 13.4 for infinitely long theta or ideal chains) has less variability over the random walks considered here than does X_1. Over all the random coil models, ideal and real, considered here (excluding therefore **C** and **Z** which are not random coils, as well as the nonconnected small-bead models and model **x** which are unphysical) X_1 has mean and standard deviation of 9.3 and 1.5, while X_2 has mean and standard deviation of 12.8 and 1.0. The relative standard deviation of X_2 is therefore about one half that of X_1. This is also obvious in Fig. 14, which displayed the distributions of $X_1/\langle X_1\rangle$ and $X_2/\langle X_2\rangle$. Therefore, X_1 is not the best candidate for an invariant dimensionless ratio combining V_h, R_g, and R_h, and we conclude that the des Cloizeaux-Weill conjecture is not supported by our results.

Another quantity characterizing the hydrodynamic properties of a particle is R_η, or the radius of the equivalent sphere that possesses the same hydrodynamic volume as the particle. Then we have

$$\frac{2}{5}V[\eta] = \frac{2}{5}m[\eta]_P = \frac{4\pi}{3}R_\eta^3 \tag{35}$$

or

$$R_\eta = \left[\frac{3m(\eta)_P}{10\pi}\right]^{1/3}. \tag{36}$$

Although this quantity is also often called a "hydrodynamic radius," we prefer the term "viscosity radius" to distinguish it from R_h. Then the ratio

$$\frac{R_\eta}{R_h} = \left(\frac{3X_2}{10\pi}\right)^{1/3} \tag{37}$$

is another scale-invariant signature of particle shape. The limit for ideal and theta chains is about 1.09. The distribution of this ratio for all the random coil models considered here (again excluding **C**, **Z**, **x**, and the nonconnected bead models) possesses a mean of 1.07 and a standard deviation of 0.03. (Being the cube root of X_2, we indeed expect its relative standard deviation to be one third that of X_2.) In fact, the comparative lack of variability in this ratio extends well beyond the class of random coils. It is exactly 1 for spheres, and we show elsewhere that it is within about 10% of unity for all shapes except rodlike or semiflexible polymers [59].

E. Expansion factors and the ratio $X_3 = \alpha_\eta^3/\alpha_R^2\alpha_h$

Expansion factors are defined in excluded-volume theory to represent the swelling of a coil relative to its size in the theta state. For example, all of the following expansion factors can be defined:

$$\alpha_R = \frac{R_g}{R_{g\theta}}, \quad \alpha_h = \frac{R_h}{R_{h\theta}}, \quad \alpha_\eta^3 = \frac{[\eta]}{[\eta]_\theta}. \tag{38}$$

In the above expressions, the subscript θ indicates the property when measured in the theta state. On the basis of renormalization-group calculations, Freed *et al.* argued that the ratio

$$X_3 = \frac{\alpha_\eta^3}{\alpha_R^2\alpha_h} \tag{39}$$

as a function of α_R will fall on a single master curve for a given polymer-solvent system independent of temperature and molecular weight [30]. We have tested this assertion by plotting all of our data for models **A**, **D**, **M**, **Q**, **T**, **Z**, and **C**, at chain lengths $N > 500$, in Fig. 15, taking model **T** as the theta state for defining each of the expansion factors. The data fall on a single curve, and it is notable that this behavior includes models **C** and **Z**, with $\alpha_R < 1$. Furthermore, for these particular models and for $\alpha_R > 1$, the ratio seems to follow the general phenomenological relation

$$\frac{\alpha_\eta^3}{\alpha_R^2\alpha_h} = X_3 = \exp[3.32(\alpha_R - 1)]. \tag{40}$$

VIII. CONCLUSIONS

Scaling arguments for the scaling behavior of the diffusion coefficient, the friction coefficient, and the intrinsic viscosity are examined computationally using a path-integration method that can readily incorporate local structure and which

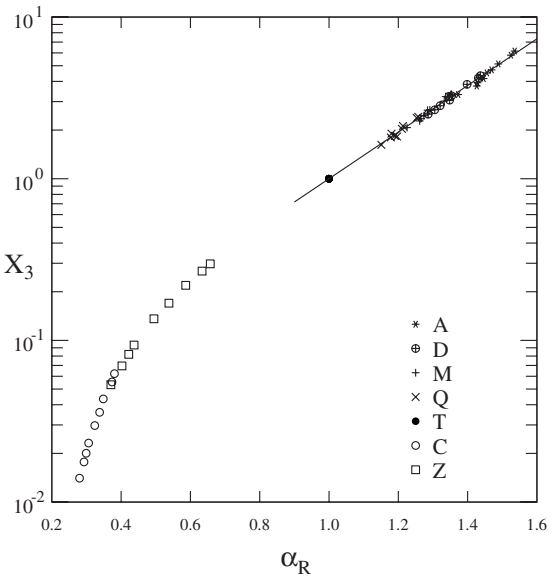

FIG. 15. The expansion factor ratio $X_3=\alpha_\eta^3/\alpha_R^2\alpha_h$ as a function of α_R is seen to lie on a single master curve for all of the indicated models. The solid line results from Eq. (35).

avoids configurational preaveraging. As often observed experimentally [19,21,22], the effective exponents for these basic solution transport properties in flexible polymers are smaller than scaling-theory estimates, while in somewhat stiffer chains, they are larger. Our calculations make it clear that polymer transport properties converge much more slowly to their asymptotic infinite-chain behavior than does R_g. In fact, the convergence is so slow, persisting to values of N as large as 10^4 that we should not expect to observe the scaling-theory estimates for the exponents in many synthetic polymers at physically accessible molecular masses.

We also assert that a long-standing explanation for this behavior, a crossover from theta to good solvent conditions, is not necessarily correct. Many of the models examined here, when short, display effective exponents for transport properties in the vicinity of 0.5, while the same effective exponents increase at larger N. But effective exponents for the radius of gyration of the same models show no similar trends, being essentially the same at small and large N. An explanation in terms of a crossover from theta to good solvent behavior can only be invoked if it is observed in the R_g data. Furthermore, any theta to good solvent crossover will almost certainly have a draining crossover superimposed upon it, and it should be difficult to separate the two effects solely on the basis of transport property measurements.

We have demonstrated that the dimensionless parameters $\Psi_h=R_h/R_g$ and $\Psi_\eta=m[\eta]_P/R_g^3$ converge, respectively, to 0.79 and to 6.6 for both ideal and for theta-state chains in the large-N limit. The limiting value of these ratios for real chains appears to depend on the balance between attractions and repulsions in the intersegmental interactions, and therefore do not converge to any particular value. This nonuniversality reflects the variation of hydrodynamic screening with solvent quality, with the screening being weaker in swollen chains.

Contrary to a conjecture made some time ago [20], we find that the ratio $\Psi_h\Psi_\eta=m[\eta]_P/R_g^2R_h$ varies appreciably from one random coil to another. A better invariant proves to be $\Psi_h\Psi_\eta^3=m[\eta]_P/R_h^3$. We also find that $R_\eta/R_h=0.457\Psi_h^{1/3}\Psi_\eta^{-1}$ is within about 5% of 1.05 for most of the random coils studied. Finally, we have confirmed that the combination of expansion factors $\alpha_\eta^3/\alpha_R^2\alpha_h$ as a function of α_R falls on a single master curve independent of the contact potential, which would be equivalent, in the laboratory, to a single master curve for a given polymer-solvent system simultaneously representing data at many temperatures and many molecular weights.

These results call into question a great deal of polymer characterization work that has been performed over the years. Because of their relative simplicity, intrinsic viscosity measurements have been extensively employed to estimate metric properties such as the characteristic ratio. Our results indicate that estimates of chain metrical properties based on transport data need to be re-examined.

ACKNOWLEDGMENT

Computational facilities were provided by the High Performance Computing Facility of Stevens Institute of Technology.

[1] J. B. Hubbard and J. F. Douglas, Phys. Rev. E **47**, R2983 (1993).
[2] J. F. Douglas, H.-X. Zhou, and J. B. Hubbard, Phys. Rev. E **49**, 5319 (1994).
[3] H.-X. Zhou, A. Szabo, J. F. Douglas, and J. B. Hubbard, J. Chem. Phys. **100**, 3821 (1994).
[4] J. F. Douglas and E. J. Garboczi, Adv. Chem. Phys. **91**, 85 (1995).
[5] H.-X. Zhou, Biophys. J. **69**, 2286 (1995).
[6] E. J. Garboczi and J. F. Douglas, Phys. Rev. E **53**, 6169 (1996).
[7] J. F. Douglas, Adv. Chem. Phys. **102**, 121 (1997).
[8] J. A. Given, J. B. Hubbard, and J. F. Douglas, J. Chem. Phys. **106**, 3761 (1997).
[9] M. L. Mansfield, J. F. Douglas, and E. J. Garboczi, Phys. Rev. E **64**, 061401 (2001).
[10] M. L. Mansfield and J. F. Douglas, Condens. Matter Phys. **5**, 249 (2002).
[11] E.-H. Kang, M. L. Mansfield, and J. F. Douglas, Phys. Rev. E **69**, 031918 (2004).
[12] M. L. Mansfield, J. F. Douglas, S. Irfan, and E.-H. Kang, Macromolecules **40**, 2575 (2007).
[13] M. L. Mansfield and J. F. Douglas, Macromolecules **41**, 5412 (2008).
[14] M. L. Mansfield and J. F. Douglas, Macromolecules **41**, 5422 (2008).

[15] M. L. Mansfield and J. F. Douglas, Phys. Rev. E **78**, 046712 (2008).
[16] P.-G. deGennes, *Scaling Concepts in Polymer Physics* (Cornell University Press, Ithaca, NY, 1979).
[17] K. F. Freed, *Renormalization Group Theory of Macromolecules* (Wiley-Interscience, New York, 1987).
[18] J. C. Le Guillou and J. Zinn-Justin, Phys. Rev. Lett. **39**, 95 (1977).
[19] M. Doi and S. F. Edwards, *The Theory of Polymer Dynamics* (Oxford University Press, Oxford, 1986).
[20] G. Weill and J. des Cloizeaux, J. Phys. (Paris) **40**, 99 (1979).
[21] M. Adam and M. Delsanti, Macromolecules **10**, 1229 (1977).
[22] P. J. Flory, *Principles of Polymer Chemistry* (Cornell University Press, Ithaca, NY, 1953).
[23] J. G. Kirkwood and J. Riseman, J. Chem. Phys. **16**, 565 (1948).
[24] H. Yamakawa, *Modern Theory of Polymer Solutions* (Harper and Row, New York, 1971).
[25] B. H. Zimm, J. Chem. Phys. **24**, 269 (1956).
[26] B. H. Zimm, G. M. Roe, and L. F. Epstein, J. Chem. Phys. **24**, 279 (1956).
[27] J. F. Douglas and K. F. Freed, Macromolecules **17**, 2344 (1984).
[28] S. Q. Wang, J. F. Douglas, and K. F. Freed, J. Chem. Phys. **85**, 3674 (1986).
[29] S. Q. Wang, J. F. Douglas, and K. F. Freed, J. Chem. Phys. **87**, 1346 (1987).
[30] K. F. Freed, S.-Q. Wang, J. Roovers, and J. F. Douglas, Macromolecules **21**, 2219 (1988).
[31] J. F. Douglas and K. F. Freed, Macromolecules **27**, 6088 (1994).
[32] P. J. Flory, *Statistical Mechanics of Chain Molecules* (Wiley, New York, 1969).
[33] See supplementary material at http://link.aps.org/supplemental/10.1103/PhysRevE.81.021803 for arguments justifying Eqs. (12), (13a), (13b), (14)–(18), and (23)–(27), and for curves displaying extrapolation of the ratios Ψ_h and Ψ_η to $N\rightarrow\infty$.
[34] A. N. Rissanou, S. H. Anastasiadis, and I. A. Bitsanis, J. Polym. Sci., Part B: Polym. Phys. **44**, 3651 (2006).
[35] M. L. Mansfield, J. Chem. Phys. **127**, 244902 (2007).
[36] N. Madras and A. D. Sokal, J. Stat. Phys. **50**, 109 (1988).
[37] B. Berg and D. Foerster, Phys. Lett. B **106**, 323 (1981).
[38] C. Aragao de Carvalho, J. Phys. (Paris) **44**, 323 (1983).
[39] C. Aragao de Carvalho, S. Caracciolo, and J. Froelich, Nucl. Phys. B **215**, 209 (1983).
[40] This method for generating rings is justified as follows. (1) Pivoting is known to generate self-avoiding linear walks without bias [36]. (2) Every unique linear walk returning to the origin constitutes one instance of a self-avoiding ring, so taking each instance of a returning linear generates rings without bias. (3) Selecting every tenth ring so generated ensures that there will be minimal correlation between successive samples—rings are so rare that many pivots are required to see ten of them. This technique may not be extremely efficient, but because our transport property calculation limits us to around 10^3 instances of any given polymer chain, the technique is adequate for our needs.
[41] The large variation in segmental volume among these models explains our decision to employ the mass-normalized version of the intrinsic viscosity. For example, at $N=1200$, the mass-normalized intrinsic viscosities of models **Ab2** and **As** differ by about 35%, while their volume-normalized intrinsic viscosities differ by a factor of about 30.
[42] E. Orlandini and S. G. Whittington, Rev. Mod. Phys. **79**, 611 (2007).
[43] J. G. Kirkwood, J. Polym. Sci. **12**, 1 (1954).
[44] B. Dünweg, D. Reith, M. Steinhauser, and K. Kremer, J. Chem. Phys. **117**, 914 (2002).
[45] J. Garcia de la Torre and B. Carrasco, Prog. Colloid Polym. Sci. **113**, 81 (1999).
[46] Y. Miyaki, Y. Einaga, H. Fujita, and M. Fakuda, Macromolecules **13**, 588 (1980).
[47] M. Schmidt and W. Burchard, Macromolecules **14**, 210 (1981).
[48] S. Park, T. Chang, and I. H. Park, Macromolecules **24**, 5729 (1991).
[49] This does not necessarily mean that one of our lattice models, adjusted to give $g=0.82$ and $C=10$ [see Eq. (11)] would be directly comparable to polystyrene. Any reasonable comparison between these lattice models and vinyl polymers would probably not assign N, the number of lattice steps, to be the same as the number of backbone bonds of the vinyl polymer.
[50] B. H. Zimm, Macromolecules **13**, 592 (1980).
[51] J. Garcia de la Torre, A. Jimenez, and J. Freire, Macromolecules **15**, 148 (1982).
[52] C. W. Pyun and M. Fixman, J. Chem. Phys. **44**, 2107 (1966).
[53] C. M. Guttman, F. L. McCrackin, and C. C. Han, Macromolecules **15**, 1205 (1982).
[54] W. Bruns, Macromolecules **17**, 2826 (1984).
[55] B. J. Cherayil, J. F. Douglas, and K. F. Freed, Macromolecules **18**, 821 (1985).
[56] B. J. Cherayil, J. F. Douglas, and K. F. Freed, J. Chem. Phys. **83**, 5293 (1985).
[57] B. J. Cherayil, J. F. Douglas, and K. F. Freed, J. Chem. Phys. **87**, 3089 (1987).
[58] X. Wang and C. Wu, Macromolecules **32**, 4299 (1999).
[59] E.-H. Kang, M. L. Mansfield, and J. F. Douglas (to be published).